Design and implementation of an improved power-electronic system for feeding loads of smart homes in remote areas using renewable energy sources

Zamanzad Ghavidel, Behnam; Maalandish, Mohammad; Hosseini, Seyed Hossein; Sabahi, Mehran; Mohammadi-Ivatloo, Behnam

Published in:
IET Renewable Power Generation

DOI (link to publication from Publisher):
10.1049/rpg2.12001

Publication date:
2021

Document Version
Publisher's PDF, also known as Version of record

Received: 18 October 2020

DOI: 10.1049/rpg2.12001

IET Renewable Power Generation

The Institution of Engineering and Technology WILEY

ORIGINAL RESEARCH PAPER

Design and implementation of an improved power-electronic system for feeding loads of smart homes in remote areas using renewable energy sources

Behnam Zamanzad Ghavidel[1] | **Mohammad Maalandish**[1] | **Seyed Hossein Hosseini**[1,2] | **Mehran Sabahi**[1] | **Behnam Mohammadi-Ivatloo**[1,3]

[1] Faculty of Electrical and Computer Engineering, University of Tabriz, Tabriz, Iran

[2] Faculty of Electrical and Computer Engineering, University of Tabriz, Tabriz, Iran

[3] Department of Energy Technology, Aalborg University, Aalborg, Denmark

Correspondence
Seyed Hossein Hosseini, Faculty of Electrical and Computer Engineering, University of Tabriz, Tabriz, Iran
E-mail: hosseini116j@yahoo.com

Abstract

This paper suggests an improved step-up step-down DC-DC system along with three-input and four-output for smart home applications. In this configuration, two unidirectional power ports have been identified as an Input power supply and one bidirectional power port for the power-saving element, which can be used as a bidirectional converter for the hybrid vehicle to discharge in a dependent structure. This system can be used to combine renewable energy sources like photovoltaic (PV), fuel cell, battery and hybrid vehicle (HV) to prepare power for remote smart homes. By using this system, serving different loads with different voltage range from high voltage to ultra-low voltage is possible, also battery charge and discharge with the energy-saving method can be achieved. In this system, the condition of all possible low-voltage load and high-voltage load conditions has been assumed. In this structure, nine power switches have been used, in which all of these switches are in control with independent and dependent duty cycles. By using these cycles, maximum power can be earned from PV sources, bus-bar voltage regulation, and battery power control is possible too. In this topology, depending on environmental conditions, five scenarios have been identified. To prove the capability of the system before the build, some valid simulations are needed. In this study, the suggested system has been simulated with power system computer aided design/electromagnetic transients including DC (PSCAD/EMTDC).

1 | INTRODUCTION

Nowadays, the demand for energy is increasing day by day. Many sources of energy achieve from fossil fuel sources. These types of fuels have many environmental issues such as a rise in temperature and consequently climate changes. Solar in photovoltaic (PV) systems is one of the most important types of clean energy sources. The main advantages of PV systems are that it is renewable, pollution-free, widespread use across the earth, long life, easy transportation, the possibility of fast installation and non-requirement of any periodic maintenance services. The main factors that are required to generate energy through PV systems are solar irradiation and temperature. The production of renewable energy from wind and sun depends on environmental conditions in the day and seasonal periods. In distributed generation through solar energy, one of the problems the system faces is the fluctuation of their output energy via changing weather conditions, which is the most important problem [1]. Additionally, the complexity is intensified if the consumption of electrical demand contaminates with uncertainty [2]. In such systems, the integration of several types of energy equipment such as electrical energy generation, energy storage systems, and renewable energy sources are defined as hybrid energy systems (HESs). Hybrid systems usually use one or more energy storage elements such as ultra-capacitors, batteries and one or more other green sources such as fuel cell (FC) or even non-renewable energy sources such as diesel generators. In general, HESs are divided into two classes of AC and DC-link systems.

In the previous years, the AC and DC coupling was investigated and had problems such as the number of electrical elements, high initial cost, large volume and difficult energy management [3, 4]. In recent years, in this approach, the tendency toward multi-input multi-output systems has been increased and several sources have been incorporated into an integrated structure. One of the advantages of these systems is the simplicity of the structure, the integrated control system, the very low cost and suitable for deploying on the low and medium power scale. In an isolated system, the input and output sources have been isolated from each other with high-weight transformers. [5]. Due to the low voltage level produced by renewable sources, it is very important to increase the system voltage level [6]. Increasing the voltage of the converter causes voltage pressure in the switches and increases losses and soft-switching is a way to overcome this issue [7]. Different ways to absorb the maximum power from renewable sources, with emphasis on PV maximum power tracking have been proposed in several studies. In [8], it is stated that with maximum power point tracking (MPPT), no control action is needed, and therefore the adjustment stage will be bypassed and the algorithm will update the stored energy at the end of the cycle as usual [8]. In [9, 10] a new multi-input multi-output system is considered to be fed using renewable sources without transformers which makes it inexpensive. It is considered an appropriate and simple control strategy. Also, a comprehensive power management algorithm has been implemented, to obtain maximum power from the PV, but the weak point of the system has been enhanced by the high duty cycle causing parasitic effects and increasing losses. In [11], an improved converter has been proposed for specific HV applications. One of the reasons that are considered as the disadvantage of HV can be a long time battery charging from charging stations, partly offset by the PV, which is considered a source of storage on the roof of the vehicle and battery as a source of storage. In this proposed structure, the sources are made individually and they collectively supply the load, and the switches are controlled independently. In [12], instead of using an FC, a wind turbine has been used for HES. In the presented model, the ability of connection to the power grid and energy exchange with the grid has also been considered and is designed by special application of light feeding on the street. In the presented model, a buck converter has been used to recharge the energy storage system. In this system, the energy management system has been taken into account so that the sources only charge the saving sources, if the generating energy of renewable sources is not sufficient enough, and are repeatedly fed through the grid, and if the generating energy is very small, the grid will also supply both the loads and the saving applications. In [13], a structure has been proposed for use in HV. In this case, an FC and an energy storage source have been used in which two outputs are considered and if there is no need to use this load, it is not possible to cut it in parallel. From the studied sources, it can be concluded that due to the low dynamics of the FC, it is better to use sources with high dynamics to have a more desirable transient system. In [14], the converter has been considered as dual-input single-output, which is investigated from PV and battery. The energy-saving system is used as a backup system during the night as well as to increase the system's reliability. In this system, it can be noted that the charging of the saved source with a given voltage has been increased, which increases the size of the energy storage element. In [15], the small-signal strategy, with independent control for each switch, is considered and the classical proportional integral (PI) controller has been used. The efficiency of the system has been studied which is 97%. Note that, in this system, it is possible to mention the recharge source with a boosted voltage, which increases the size of the saving energy element. In [16], the converter has been designed to use solar arrays connected to the grid. By considering two arrays as input, all of the switches and energy only flows from sources to the load without saving element. In [17], the load as a generator has the ability to charge the battery and is also applied in energy management of priority strategy. The parallel diodes have to consider a larger amount due to the bypass route which is not economical and voltage control is easier than the parallel state. In [18], a multi-input multi-output converter has been investigated. The converter is designed particularly for HVs. All inputs are unidirectional and the storage section is bidirectional as well as the sources can be shared, jointly. This converter can be used in increasing and decreasing modes. The battery is charged using the boost side which increases the size of the battery. In [19], a multi-input multi-output converter has been introduced, which is suitable for HV systems. It has been designed as an island in the output of the converter, a DC link that is placed to connect to a DC motor. In this converter, it is proposed to switch to the battery in a brake mode. Several scenarios have been considered to be used as one of the most appropriate scenarios for this study such as charging the battery by a DC motor-generator and the PV source. For proper operation of the mentioned converters, energy management should be done in accordance with different hours and seasons of the year. In [20, 21], practical and applied projects have been done. One of the best methods of energy management in a smart home with the ability to connect an electric car has been stated in [22] in which the electronic power converter is first presented, and then energy management is addressed. Electromagnetic control (EC) is a complex control system and the amount of electromagnets requires wider power. This study has tried to propose a new improved structure of energy management for use in smart homes away from the grid, and energy management in the smart home and the amount of energy production during 24 h are briefly stated.

2 | PROPOSED TOPOLOGY

In this study, a three-input and four-output DC-DC system is proposed for the hybrid system equipped with PV, FC and battery, and its general architecture is introduced in Figure 1. This system has seven ports with three-input and four-output ports. At the output ports, four levels of standard voltage for various uses are provided, including three ports, one port for PV array, the other for FC port and another one for the battery port that can transmit power. This set of converters can feed independently/dependently on the demand of the load required. This model also has a bidirectional load that has connection capability that is considered as an HV. The converter consists of nine independent and dependent switches, which are

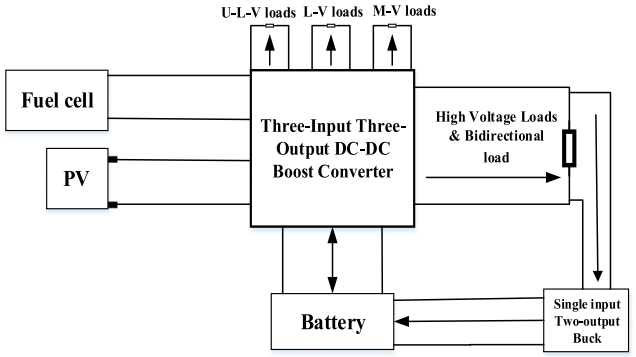

FIGURE 1 The architecture of converters and sources proposed for smart home

individually controlled by nine different duty cycles. In this study, the possibility of extracting maximum power from PV sources, regulating the power of the FC and charging and discharging the battery can be done easily. In Figure 1, the overall topology of the proposed converter is shown to be carried out on a power management battery using a PV source and bidirectional load of the HV installed at the high-voltage section of the circuit, and it can be considered the role of the backup system for the battery. In this study, two different features with different characteristics are introduced. First, the analysis of each of the converters' structures has been studied, and then the accuracy of the integrated circuit performance is investigated in the next sections.

3 | FIRST CONVERTER

The structure of the boost DC-DC converter has been proposed in Figure 2. As it is observed, the converter has two PV and FC input in two separate ports and a bidirectional port to save power. L_1 and L_2 convert the voltage source into a current source that makes the DC flow from renewable sources of PV and FC. R_{out} is representative of high voltage parallel loads and voltage source at the output as an HV and is capable of charging, discharging, or even power generation by energy generation sources such as FC and electrical motor. T_1 to T_5 are the main elements that can handle power flow on high-voltage loads and batteries. In this topology, the switches are controlled independently with five independent duty cycles. According to this strategy, the MPPT from the PV source is designed first to manage the output power of the PV, and second, to demonstrate how to charge and discharge battery power, power load management and output voltage scaling. The proposed structure also makes it possible to store the power in the battery by an HV, which a backup source for low voltage and high-voltage loads is considered for overload modes during day and night.

The proposed structure, like the conventional boost converter, converts the power flow through T_1 and T_2, and the battery will always be attached to the mid-voltage bus, which helps operate mid-voltage regulation. Moreover, the battery can use the HV source to charge. If the PV is not capable of sufficient ability during the night or overload, it is possible to enable a connection to sensitive loads using the battery. Based on these descriptions, in this study, five scenarios are proposed.

3.1 | First scenario

In the first scenario, it is assumed that the tilt of solar irradiance and PV are in the best conditions and no load is connected to the system. In this case, the battery is charged by PV without entering the second section. T_1 is switched on ($0 < t < d_1 T$) and L_1 is charged by the PV (Figure 3(a)), then T_1 is switched off and T_3 is switched on ($d_1 T < t < d_3 T$) (Figure 3(b)), and the energy stored in L_1 through T_3 is stored in the battery.

In this scenario, current and power equations charge mode in the battery can be obtained as follows:

$$I_{bat} = d_3 I_{L1} \tag{1}$$

$$P_{bat} = (d_3 I_{L1}) V_{bat} \tag{2}$$

As can be seen, in this case only the L_1 is charging and discharging. In Figure 8(a), the method of switching and comparison of the referenced and carrier signals, as well as the method of charging and discharging of L_1 has been presented.

3.2 | Second scenario

In the second scenario, it is assumed that the air temperature and light intensity are in good conditions and the PV is capable of supplying all the required loads and extra power is saved in the battery. In this case, L_1 is charged by the PV through T_1 during ($0 < t < d_1 T$) as shown in Figure 4(a). During ($d_1 T < t < d_3 T$)

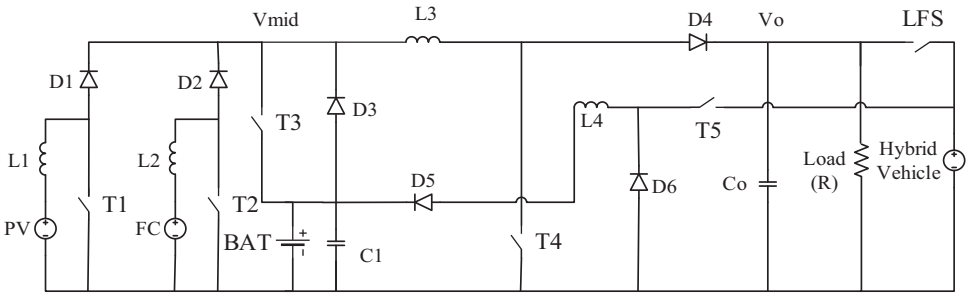

FIGURE 2 Structure of cascade boost converter

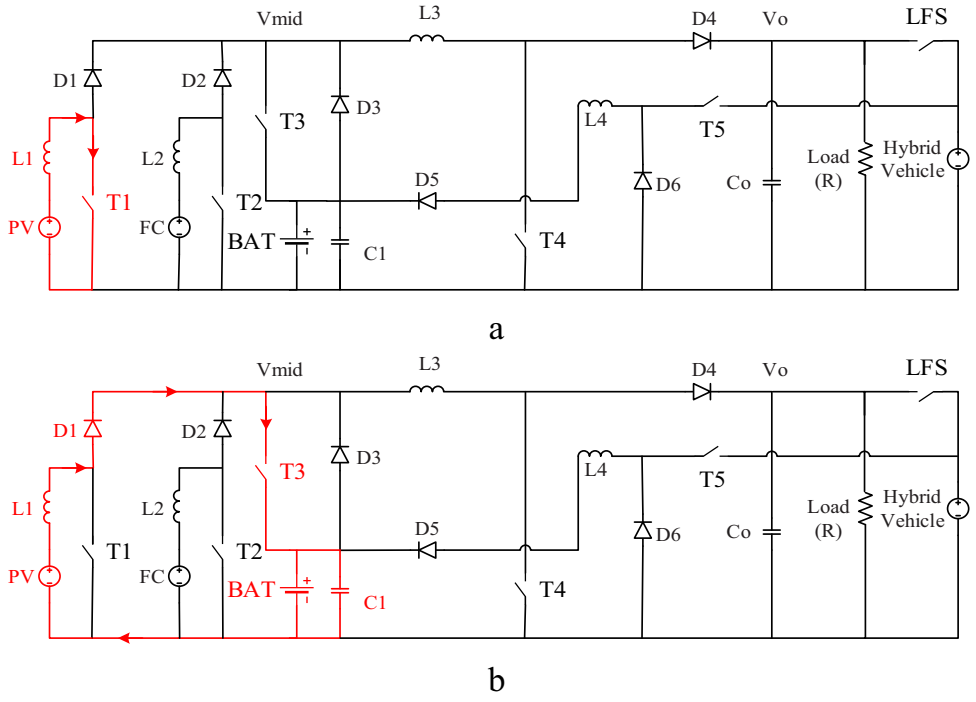

FIGURE 3 (a) The charging of the L_1 through the photovoltaic (PV), (b) battery charge by PV

T_1, T_3 and T_4 are on, the battery is charged through T_3 by mid-voltage level and L_3 is also charged through the T_4 switch of the L_3 by the mid-voltage level as shown in Figure 4(b). Finally, during $(d_4T < t < T)$ T_4 is switched off and the energy stored in L_3 flows into the load, and T_3 also remains on until the end of the period so that the battery charge could be completed fully (Figure 4(c)).

In the battery, assuming that T_3 is on

$$I_{bat} = d_3 I_{L1} - d_4 I_{L3} \tag{3}$$

$$P_{bat} = (d_3 I_{L1} - d_4 I_{L3}) V_{bat} \tag{4}$$

For the second boost section

$$V_O = \left(\frac{1}{1-d_4}\right)\frac{1}{1-d_1} V_{pv} \tag{5}$$

$$I_O = (1-d_4)1 - d_1 I_{pv} \tag{6}$$

In Figure 8(b), the switching and comparison of the reference and carrier signal, as well as the charging and discharging of the L_1 and L_2 signals, are expressed.

3.3 | Third scenario

In the third scenario, with the assumption of night, the PV is not capable of producing energy, so the output power is supplied only by the FC and battery. The HV does not need to be charged or needs discharging. In this case, during $(0 < t < d_2T)$, L_2 and L_3 are charged by the FC and battery. In Figure 5(a), the battery also plays the role of stabilising the mid-voltage section. In the second case, during $(d_2T < t < T)$ T_2 is switched off and the energy stored in L_2 is directed toward L_3. Also, in Figure 5(b), the battery charge could be completely discharged to L_3, and the energy stored in L_2 is inserted into L_3. Finally, during $(d_4T < t < T)$, the total energy that is charged in L_3 by battery and FC are discharged into the load (Figure 5(c)).

The total energy stored in the battery, charged by the PV and the HV, is discharged into the loads:

$$I_{mid} = (1-d_2) I_{fc} + I_{bat} \tag{7}$$

$$I_{bat} = (d_1) I_{L1} \tag{8}$$

$$P_{bat} = (d_1 I_{L1}) V_{bat} \tag{9}$$

$$V_O = \left(\frac{1}{1-d_4}\right)\frac{1}{1-d_2} V_{fc} \tag{10}$$

$$I_O = (1-d_4)(1-d_2) I_{fc} + I_{bat} \tag{11}$$

In Figure 8(c), the switching and comparison of the reference and carrier signal as well as the charging and discharging of L_2 and L_3 signals are expressed thoroughly.

3.4 | Fourth scenario

In this scenario, it is assumed that during the daytime, the system is facing overload, and all sources including PV, FC, battery and HV are online and feed the mid-voltage section to supply

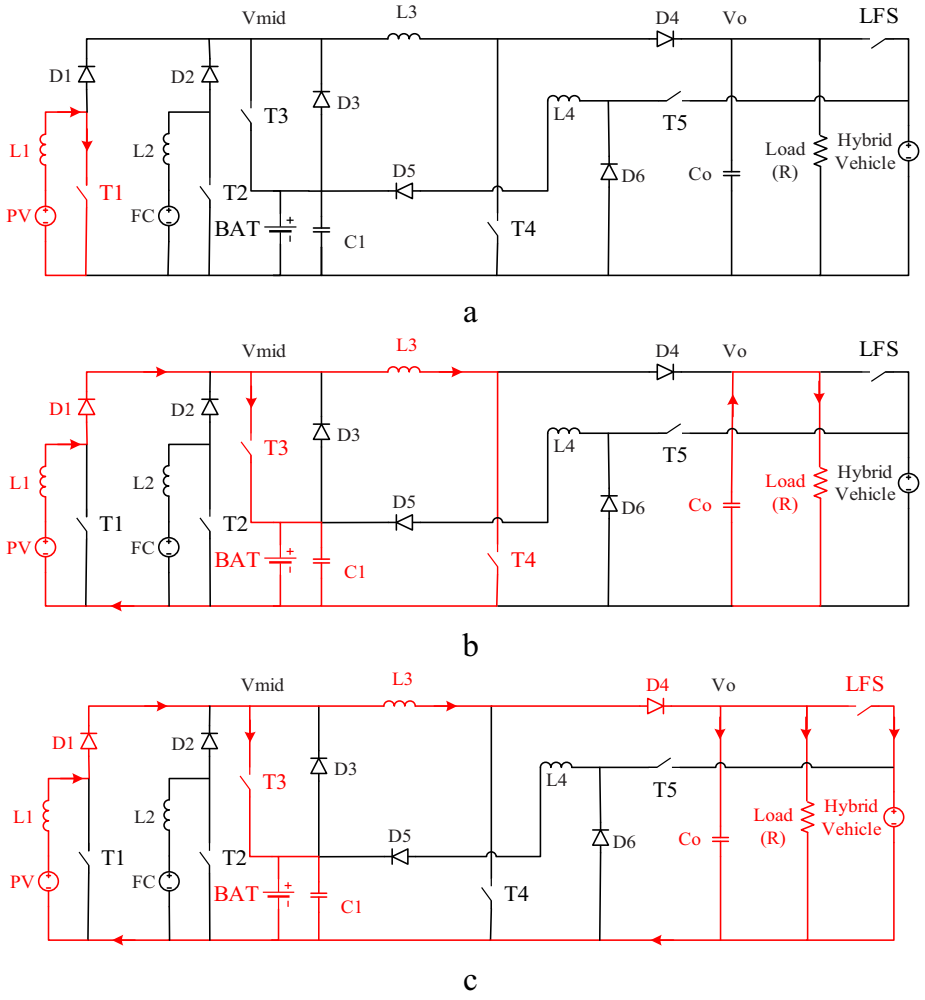

FIGURE 4 (a) Charging the L_1 by the PV, (b) charging the battery by PV, (c) L_3 feed the output loads

the high-voltage and low-voltage sections. In the first case, all switches are on at the same time, L_1 is charged by PV and L_2 is charged by FC, as well as L_4 transfers the energy from the HV to the battery during $(0 < t < d_1 T)$ as shown in Figure 6(a). During $(d_1 T < t < T)$, T_1 is switched off and the energy stored in L_1 is directed toward L_3, the battery charge could be completely discharged to L_3, and L_2 is still charged from the FC because of the low dynamics of the FC (Figure 6(b)). Then, during $(0 < t < d_2 T)$, T_2 is switched off and the energy stored in L_2 is directed toward L_3 and the total energy that is charged in L_3 by battery, PV and FC are discharged into the load (Figure 6(c)). In the fourth mode, energy is stored in L_3, and during $(d_4 T < t < T)$, T_4 is switched off and the energy stored in L_3 is directed toward the load (Figure 6(d)). On the other hand, the hybrid energy compensated by the battery depletes battery energy in L_3. During $(d_5 T < t < T)$, the total energy that is charged in L_5 by HV is discharged into the battery, which has a backup role (Figure 6(e)).

It is observed in the FC:

$$V_{bat} = V_{mid} = \frac{1}{1 - d_1} V_{pv} = \frac{1}{1 - d_2} V_{fc} \tag{12}$$

In this case, the voltage of mid-voltage is fed by PV, FC and battery and the battery also has a regulator role for mid-voltage section

$$V_{bat} = d_5 V_{byb} \tag{13}$$

$$I_{byb} = d_5 I_{bat} \tag{14}$$

The method of switching and comparison of the reference signal and charging and discharging of L_1, L_2, L_3 and L_4 is expressed in Figure 8(d).

3.5 | Fifth scenario

In this scenario, it is assumed that during the night, the system is faced with an overload and all the input sources except PV are online, which in this case the HV is fed to the battery by buck converter which causes the battery to be charged and the level of the mid-voltage section is stabilised. In the first case, during $(0 < t < d_2 T)$, L_2 and L_3 are charged by FC and battery (Figure 7(a)). Then, during $(d_2 T < t < T)$, T_2 is switched off

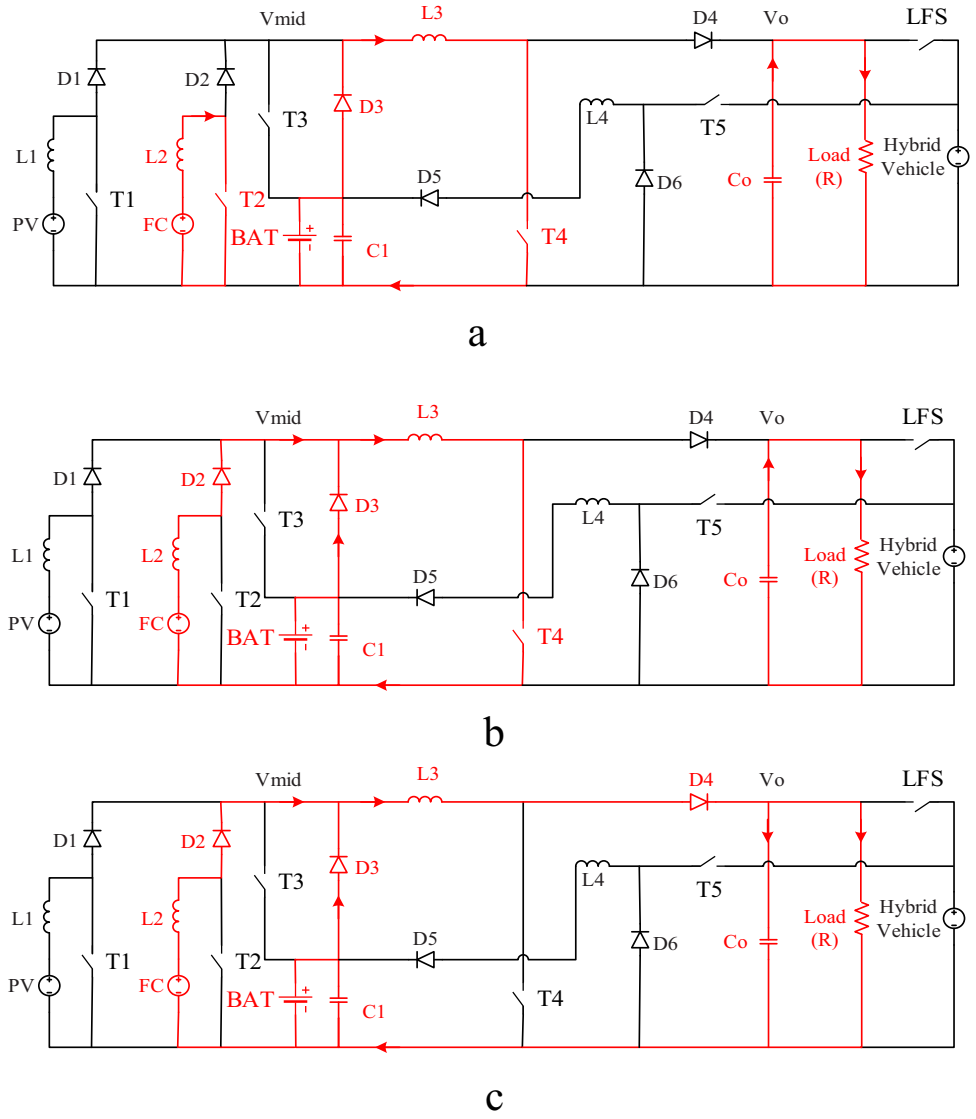

FIGURE 5 (a) L_2 is charged by the FC and L_3 is charged by the battery, (b) L_3 is charged by battery and L_2, (c) L_3 feeds the output loads

and the energy stored in L_2 is directed toward L_3. Also, the battery charge could be completely discharged to L_3 (Figure 7(b)). In the next step, during ($d_4T < t < T$), the total energy that is charged in L_3 by battery and FC are discharged into the load (Figure 7(c)).

In the end step, during ($d_5T < t < T$), the total energy that is charged in L_5 by HV is discharged into the battery (Figure 7(d)).

The fifth scenario equations as follows:

$$V_{bat} = d_5 V_{hyb} \tag{15}$$

$$I_{hyb} = d_5 I_{bat} \tag{16}$$

$$V_O = \left(\frac{1}{1-d_4}\right)\frac{1}{1-d_2} V_{fc} \tag{17}$$

$$I_O = (1-d_4)(1-d_2) I_{mid} + I_{bat} \tag{18}$$

The method of switching and comparison of reference and output signals as well as the charging and discharging mode of L_2, L_3 and L_4 have been expressed in Figure 8(e).

4 | SECOND CONVERTER

The structure of the DC-DC buck converter single-input two-output is proposed, which is shown in Figure 9. As it is observed, the converter has a DC input that is produced at the output of two voltages of medium and ultra-low voltage.

This converter is used to provide medium voltage and ultra-low-voltage loads to use in applications such as lighting, security systems and monitoring as well as ultra-low voltage such as smart phones, phones and control systems. In this converter, two proposed voltage levels are adjusted according to the international standards for electrical installation (ICE) standard,

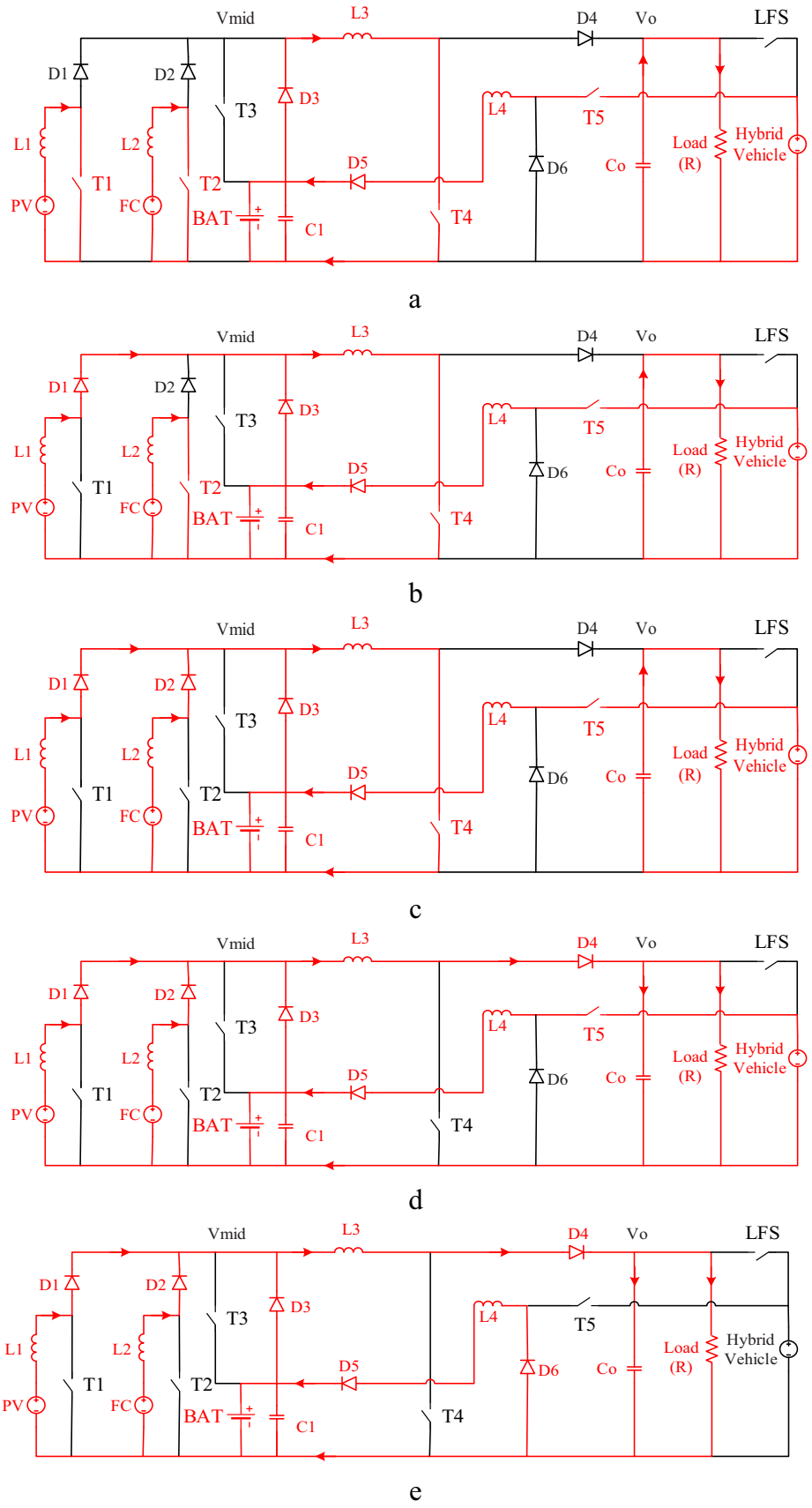

FIGURE 6 (a) L_1 by PV, L_2 by the FC and L_3 by battery are charged, also battery is charged by HV, (b) L_3 is charged by battery and L_1, also battery is charged by HV, (c) L_3 is charged by battery, L_1 and L_2, also battery is charged by HV, (d) L_3 feeds the output loads, (e) T_5 switched off and battery charge could be completed

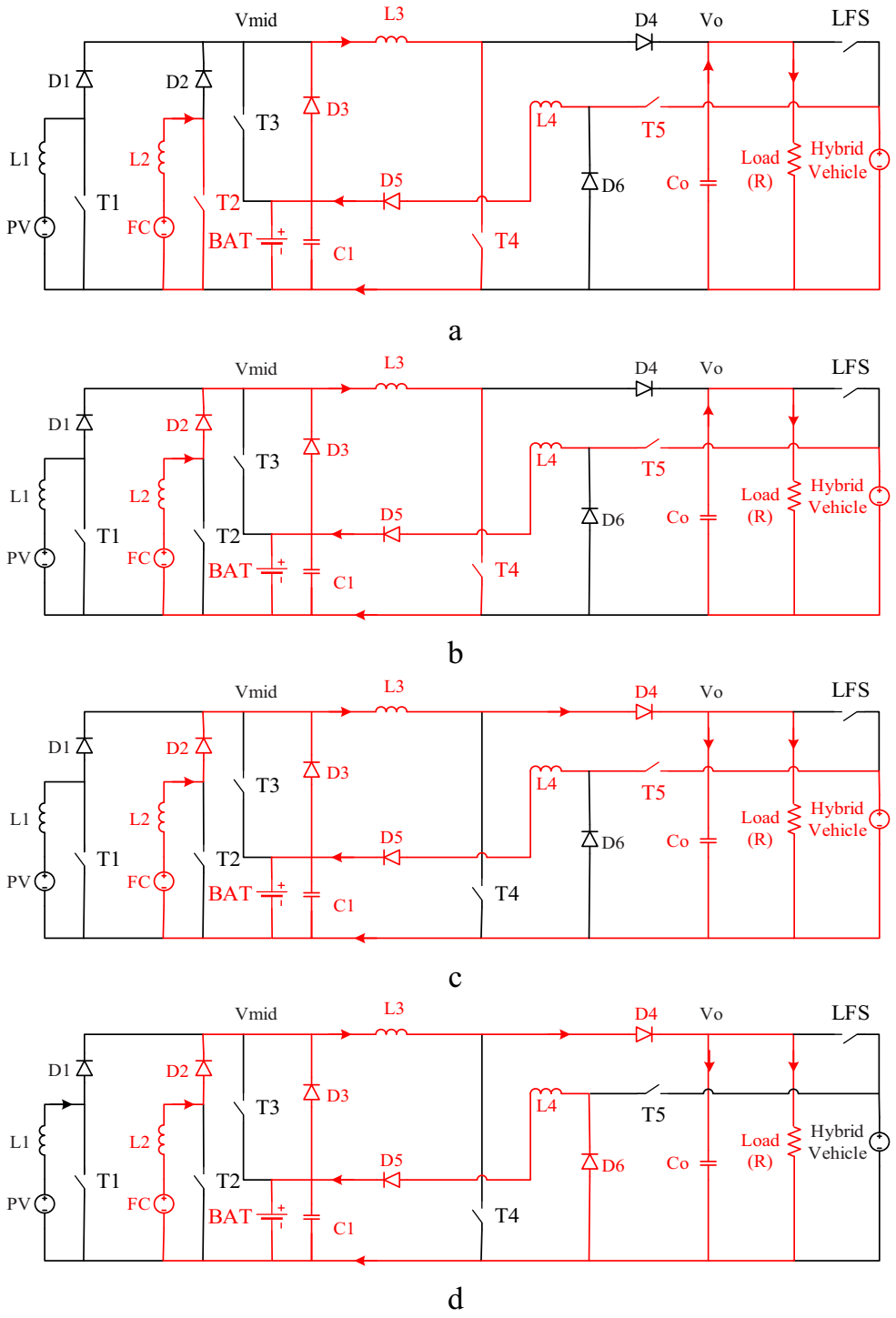

FIGURE 7 (a) L_2 by the FC and L_3 by battery are charged, also battery is charged by HV, (b) L_3 is charged by battery and L_2, also battery is charged by HV, (c) L_3 feeds the output loads, (d) T_5 switched off and battery charge could be completed

where the converter input from the previous converter switch is split in parallel and can be used if problems arise from the previous system's storage source. This converter is considered to be identical with the switching frequency but can be achieved by changing the duty cycle to different voltages based on the need. As shown in Figure 9, L_2, L_5 and L_6 can be integrated into three heads to be able to feed very low loads using two capacitors and a very small inductance, as well as a step-down gain. According to the calculations done in the duty cycle, 0.5 is reduced to 30 times the voltage. As can be seen, the V_{mid} is first received from the previous circuit and enters L_5, via T_6, and some of the energy is lowered into the voltage by T_7 and is reduced to very low-voltage loads after the buck is passed. As shown in the topology, by changing the free circulation phase of

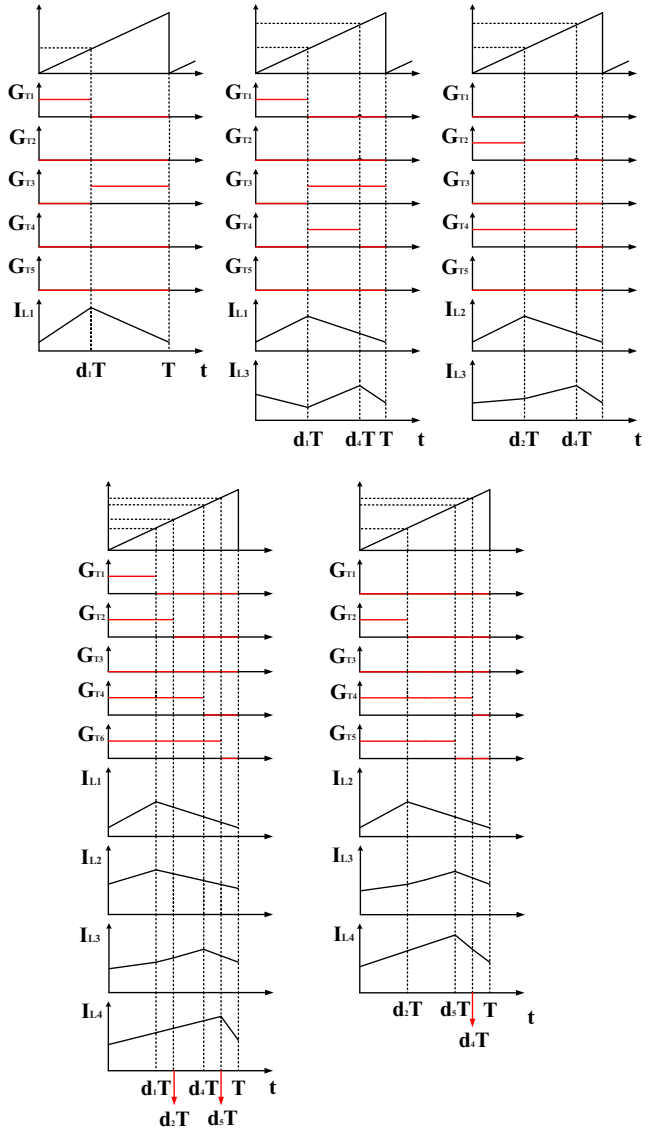

FIGURE 8 Plot of switching and current-time diagram of all scenarios

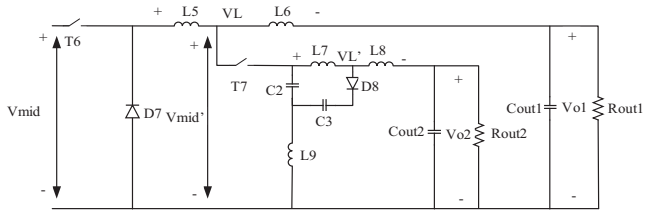

FIGURE 9 Topology of the single-input two-output converter

a conventional buck converter and adding two very small capacitors and inductors, the input-voltage level significantly reduced the input-voltage level.

Assuming ohmic loads and same frequency and assuming T_6 is on:

$$V_L = (V_{mid} - V_{O1} - V_L - E_{step\_down})d_6 T \tag{19}$$

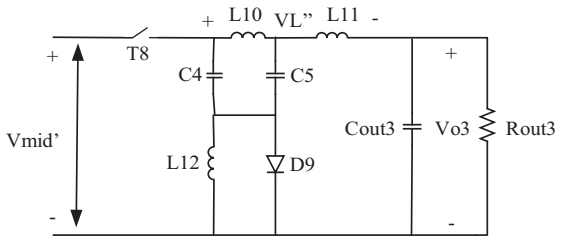

FIGURE 10 Single-input single-output buck topology reducing the voltage and current ripple

Assuming the T_6 is off:

$$V_{O1} = \frac{2}{3} V_{mid} d_6 \tag{20}$$

For very ultra-low voltage:

$$V_{mid'} = V_{mid}\left(1 - \frac{1}{2}d_6\right) - \frac{1}{2}V_{O1}d_6 \tag{21}$$

Assuming T_7 is on:

$$V_{mid'} = V_{C1} + V_{L5} \tag{22}$$

Assuming the same inductance:

$$V_L' = \left(V_{mid}\left(1 - \frac{1}{2}d_6\right) - \frac{1}{2}V_{O1}\right)d_7 \tag{23}$$

Assuming T_7 is off:

$$V_L' = (V_{C2} + V_{L9} - V_{O2}) \tag{24}$$

$$V_{mid}\left(1 - \frac{1}{2}d_6 - \frac{2}{3}{d_6}^2\right) + V_{C2}(d_7 - 1) + V_{L9}(d_7 - 1) + V_{O2}(1 - d_7) = 0 \tag{25}$$

$$V_{O2} = K{d_6}^2 d_7 V_{mid} \tag{26}$$

5 | THIRD CONVERTER

The proposed single-input single-output DC-DC converter structure is shown in Figure 10. As it is clear, the converter has a DC input that aims to reduce voltage ripple and current at low voltage output. The switch has been considered the same in the switching frequency, but it can be achieved by changing the duty cycle to the difference voltage. As shown in Figure 10, L_{10} and L_{11} can be split open with the middle head so that the low loads can be fed using two capacitors and a small inductance, as well as a buck, which is calculated.

Assuming the T_8 is on:

$$V_{mid'} = V_{mid} - V_{L5} \tag{27}$$

$$V_{mid'} = V_{C4} + V_{L12} \tag{28}$$

$$V_{L5} = \left(\frac{V_{L5} - V_{O1}}{2}\right)d_6 \tag{29}$$

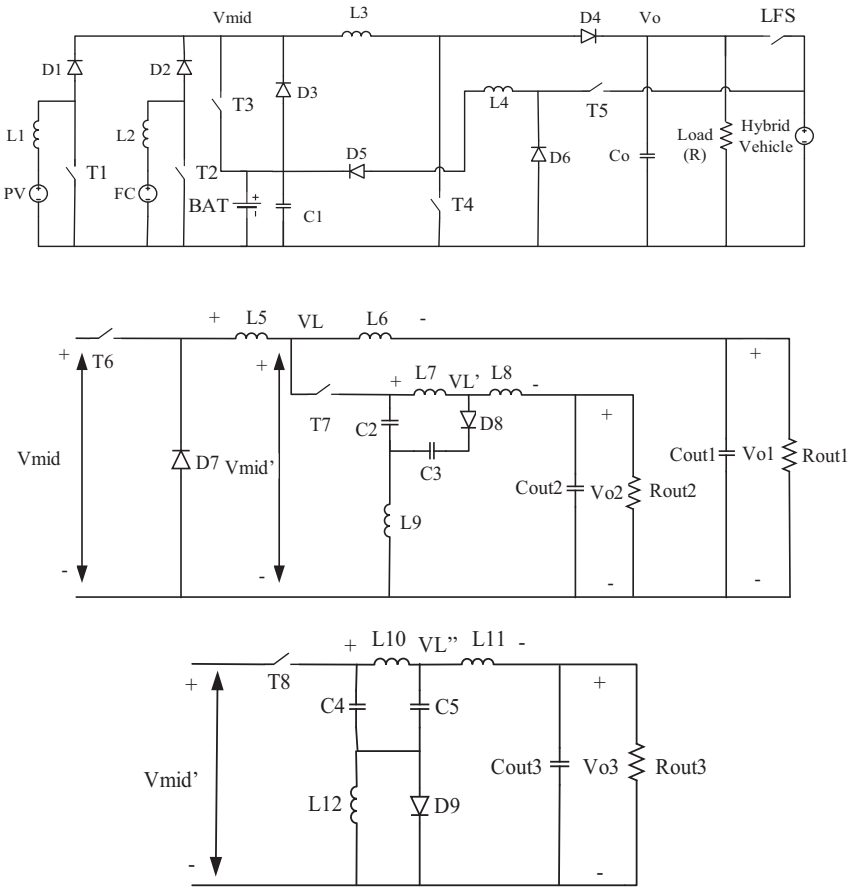

FIGURE 11 The general topology is shared by putting all resources and consumers together

$$V_L'' = \left(V_{mid}\left(1 - \frac{1}{2}d_6\right) - \frac{1}{2}V_{O1}\right)d_8 \tag{30}$$

Assuming T_8 is off:

$$V_{mid'}\left(1 - \frac{1}{2}d_6 - {d_6}^2\right) + V_{C4}(d_8 - 1) + V_{L12}\left(d^{\frac{2}{3}}{}_8 - 1\right) + V_{O3}(1 - d^{\frac{2}{3}}{}_8) = 0 \tag{31}$$

In the end, the output voltage of the lower voltage equation is obtained as

$$V_{O3} = K' {d_6}^2 d^{\frac{2}{3}}{}_8 V_{mid} \tag{32}$$

The topology is integrated into the form of three converters in parallel in Figure 11.

As can be seen, in the proposed system, more switches are used, but considering goals such as the simultaneous use of the system in boost and buck mode, several voltage levels of charging and charging of the HV as a source is negligible.

To investigate the losses of switching and the loss related to the resistance of each of the elements that are represented by P_{SW} and P_{cond}, total losses of the system are presented by P_{total}.

$$P_{total} = P_{SW} + P_{cond}$$

To simplify the calculations, the loss of capacitors is neglected ($r_c = 0$) and only the loss of resistance, the internal resistance of the sources, diodes, switches and inductances in the conduction mode are investigated:

$$P_{cond,S_i} = r_{S_i}.(I_{S_i,rms})^2 \tag{33}$$

$$P_{cond,L_i} = r_{L_i}.(I_{L_i,rms})^2 \tag{34}$$

$$P_{cond,D_i} = [V_{Fd,D_i}.I_{D_i,ave}] + \left[r_{D_i}.(I_{D_i,rms})^2\right] \tag{35}$$

$$P_{cond,T_i} = [V_{Fd,T_i}.I_{T_i,ave}] + \left[r_{T_i}.(I_{T_i,rms})^2\right] \tag{36}$$

$$P_{cond} = P_{cond,S_i} + P_{cond,L_i} + P_{cond,D_i} + P_{cond,T_i} \tag{37}$$

In order to investigate the switching losses, the uncontrollable and controllable switches should be investigated in two cases. In addition, the diodes and the switches must first be studied in light of the voltage of the diodes and the switches, which are shown with the peak inverse voltage (PIV) under the t_{on} under and t_{off} state and finally to the system efficiency relations [13]:

$$P_{SW,D_i} = \frac{1}{6}(V_{PIV,D_i})(f_S)(I_{ave,on})(t_{on} + t_{off}) \tag{38}$$

$$P_{SW,T_i} = \frac{1}{6}(V_{PIV,T_i})(f_S)(I_{ave,on})(t_{on} + t_{off}) \tag{39}$$

$$P_{SW} = P_{SW,D_i} + P_{SW,T_i} \tag{40}$$

TABLE 1 Comparison between the proposed structure and other structures

Reference	Input port	Bidirectional port	Output power delivery	Number of switches	Number of Diodes	Buck & boost (same time)	Connecting hybrid vehicle ability	Output voltage level	Efficiency (average)
[9]	2	✓	Medium	4	4	Boost	Only charge	1	80%
[11]	2	✓	Medium	4	5	Boost	Only charge	1	85%
[12]	2	✓	High	4	3	Boost	Only charge	1	—
[13]	N	✓	Medium	N + M + 1	N+M+1	Boost	Only charge	M	~80.5%
[14]	1	✓	Medium	3	3	Boost	Only charge	1	~98%
[15]	N	✓	Medium	N + 1	N	Boost	Only charge	1	~97%
[16]	2	✗	Medium	2	2	Boost	Only charge	1	—
[17]	N	✓	Medium	N + 3	N	Buck	Only charge	1	~92%
[18]	N	✗	Medium	N + 2	N	Buck Or boost	Only charge	1	—
[19]	1	✓	Medium and low	4	5	Boost	Charge and discharge	1	~90.2%
Proposed	2	✓	Medium and low	8	9	Both	Charge and discharge	4	~91.53%

$$P_{Loss} = P_{cond} + P_{SW} \tag{41}$$

$$P_{out} = V_o I_o + V_{o1} I_{o1} + V_{o2} I_{o2} + V_{o3} I_{o3} \tag{42}$$

$$P_{in} = P_{out} + P_{Loss} \tag{43}$$

$$\eta = \frac{P_{out}}{P_{in}}.100 = \frac{P_{out}}{P_{out} + P_{Loss}}.100 \tag{44}$$

The efficiency and efficiency of the proposed method in the third scenario are:

$$P_{Loss} = P_{cond} + P_{SW} = 1149.195W \tag{45}$$

$$P_{out} = V_o I_o + V_{o1} I_{o1} + V_{o2} I_{o2} + V_{o3} I_{o3} = 9807 \tag{46}$$

$$\eta = \frac{P_{out}}{P_{in}}.100 = \frac{P_{out}}{P_{out} + P_{Loss}}.100 = \frac{9807}{10956.195} = 89.5\% \tag{47}$$

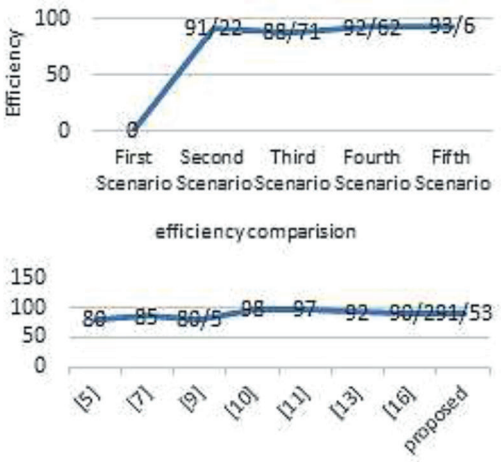

FIGURE 12 (a) Comparison efficiency between proposed system and other topologies, (b) comparison of the system efficiency in different scenario

In Table 1, a comparison is made between the proposed hybrid system and other structures. As is observed, the proposed system has some advantages and disadvantages compared to other topologies. Also, in Figure 12(a), the comparison efficiency between the proposed system and other topologies is presented, and in Figure 12(b), the comparison of the system efficiency in different scenarios is also performed.

6 | ENERGY FLOW CONSIDERING IN THE ISLANDED HOME

Using the stated topics, a smart house can be considered as an island by determining the minimum and maximum load. In this case, by examining the loads used in smart homes, the input sources can be evaluated and measured. In Figure 13, power flow in the system and the connection between the hybrid vehicle and the converter are schematically represented. Also, Figure 14 shows the evaluation of the power generation during 24 h. In Table 2, the method of production and consumption of power in different scenarios is summarised.

7 | SIMULATION AND EXPERIMENTAL RESULTS

In this section, the simulation and experimental works are provided for verifying the operation of the proposed system.

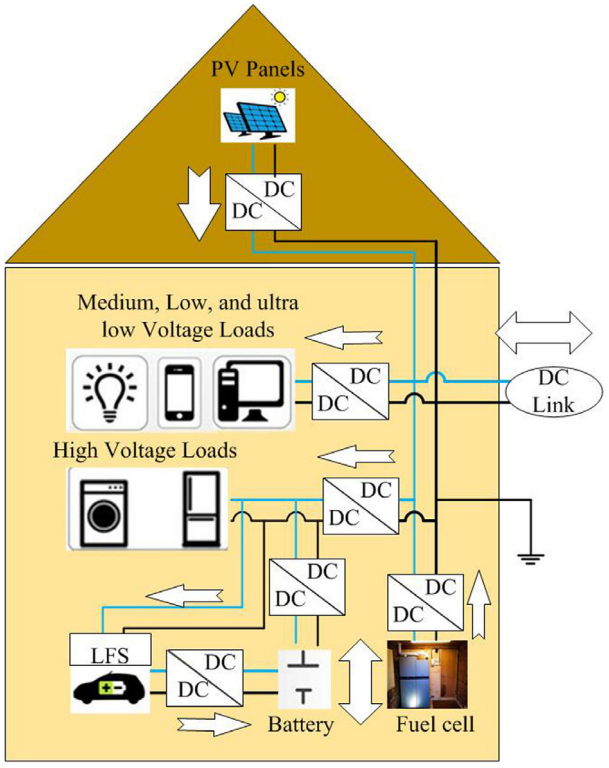

FIGURE 13 Power flow in smart home

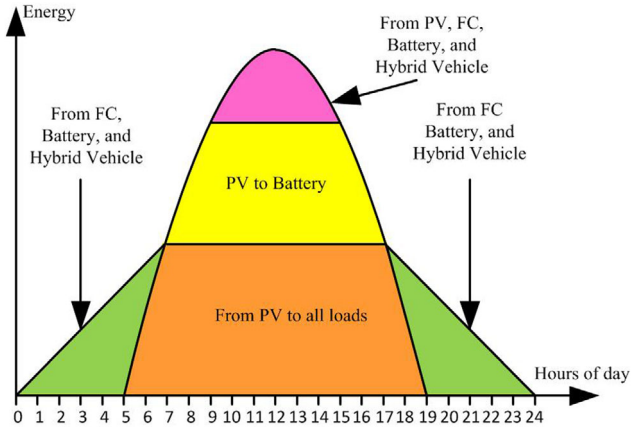

FIGURE 14 Evaluation of the power generation during 24 h

TABLE 3 The values of the parameters

Symbols	Parameters
$L_1 = L_2 = L_4$	1000
L_3	2000
C_1	2000
C_{out}	3000
R_{load}	1~2
R_{int}	0.1
$L_5 = L_6$	500
$C_2 = C_4 = C_5$	10
$L_7 = L_8 = L_{10} = L_{11}$	250
L_9	20
C_3	10
$C_{out}1$	500
$C_{out}2 = C_{out}3$	200
$R_{o}1$	3
$R_{o}2$	5
$R_{o}3$	4

Simulation works are done using the PSCAD/EMTDC software. The prototype of the experiment at different duty cycles and power rated is of almost 25 kW. Also, the used parameters in the proposed system are provided in Table 3.

Figure 15 indicates the simulation waveforms of the high voltage section. Figure 15(a) illustrates that the value of the output of the high-voltage section is about 230 V, and after step-change at the system loads, the system voltage is regulated to 230 V again after the voltage drops. Also, the values of the other parameters are P_{high} = 24 kW, I_{high} = 101 A as shown in Figures 15(b) and (c), and the waveform of L_3's voltage and current are illustrated in Figures 15(d) and (e). Also, the waveform of T_4's voltage and current are illustrated in Figures 15(f) and (g). Figure 16 indicates the simulation of the medium-voltage section. Figure 16(a) illustrates that the value of the output of the medium-voltage section is about 52 V and after step-change at the system loads, the system voltage is regulated to 50 V. In this part, a voltage drop of 4% is observed and its effect on the current and power of the part is observed in Figures 16(b) and (c). The values of the parameters are P_{medium} = 1.25 kW and I_{medium}

TABLE 2 Power flow at the system

Balance between production and consumption	Explanation
$P_{load} = 0 \& P_{pv} = P_{bat}$	First scenario: There are no load in the smart home, and in this scenario, all energy generated in the photovoltaic (PV) array is stored in the battery
$P_{pv} = P_{Load} + P_{bat} + P_{hyb}$	Second scenario: The power generated in the PV array divided between battery, load and hybrid vehicle.
$P_{fc} + P_{bat} = P_{load}$	Third scenario: In the absence of hybrid vehicle and during the night, energy production of fuel cell and energy stored in the battery is used.
$P_{pv} + P_{fc} + P_{bat} + P_{hyb} = P_{load}$	Fourth scenario: In this condition, system is faced with overload during daytime and all sources product energy for loads.
$P_{pv} = 0 \& P_{fc} + P_{bat} + P_{hyb}$	Fifth scenario: In this condition, system is faced with overload during night time and all sources, except PV array, product energy for loads

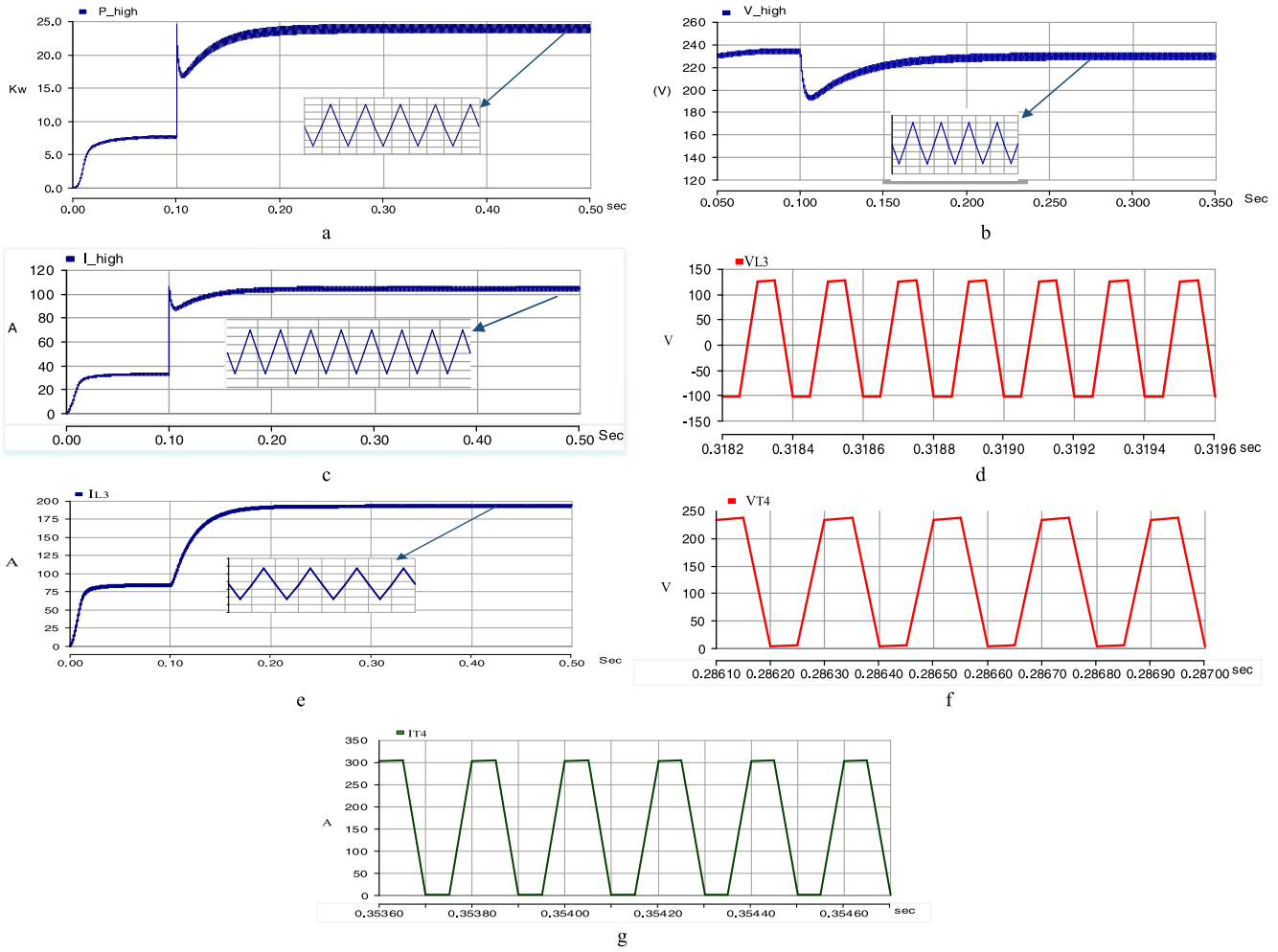

FIGURE 15 (a) High-voltage section's voltages in step-change mode, (b) power delivery for the high-voltage section in step-change mode, (c) high-voltage section's current in step-change mode, (d) L_3's voltage in steady-state mode, (e) L_3's current in step-change mode, (f) T_4's voltage in steady-state mode, (g) T_4's current in steady-state mode

= 25 A. Also, the waveform of L_6's current and T_6's voltage and current are illustrated in Figures 16(d) to(g).

Figure 18 indicates the experimental results of the system. Figure 18(a) illustrates that the value of the output of the medium-voltage section is about 57 V and it matches with Figure 16(a). The difference between the two waveforms is about 8.7%. Figure 18(a) illustrates that the value of the output of the medium-voltage section is about 57 V and it matches with Figure 16(a). The difference between the two waveforms is about 8.7%. Figure 18(b) illustrates that the value of the output of the low-voltage section is about 18.6 V and it matches with Figure 16(a). The difference between the two waveforms is about 22%. Unfortunately, it should be noted that this difference is a bit large. Figure 18(b) illustrates that the value of the output of medium-voltage current is about 28 A and it matches with Figure 16(c). The difference between the two waveforms is about 10%. Figure 18(c) illustrates that the value of the output of ultra-low-voltage current is about 4 A it matches with Figure 17(c). The difference between the two waveforms is about 0% and they completely match. Finally, Figures 18€ and (f) are relatively consistent with Figures 16(e) to (g) and 15(e).

Figure 17 indicates the simulation of the low and ultra-low-voltage sections. Figure 17(a) illustrates that the value of the output of the low-voltage section is about 14.2 V and after step-change at the system loads, the system voltage is regulated to 13.8 V. In this part, a voltage drop of 2.8% is observed in Figure 17(a). Also, for the ultra-low-voltage section, Figure 17(b) illustrates that the value of the output of the ultra-low-voltage section is about 5.1 V and after step-change at the system loads, the system voltage is regulated to 5 V. In this part, a voltage drop of 2% is observed. The values of the parameters are $P_{ultra\text{-}low\text{-}voltage}$ = 20 W and $I_{ultra\_low\_voltage}$ = 4 A, and its effect on the current and power of the part is observed in Figures 17(c) and (d). Also, the waveform of T_8's voltage is illustrated in Figure 17(e). To evaluate the simulation results and experimental results, the prototype is built, based on this it is observed by adapting the laboratory and simulation results that there is a slight difference with acceptable accuracy.

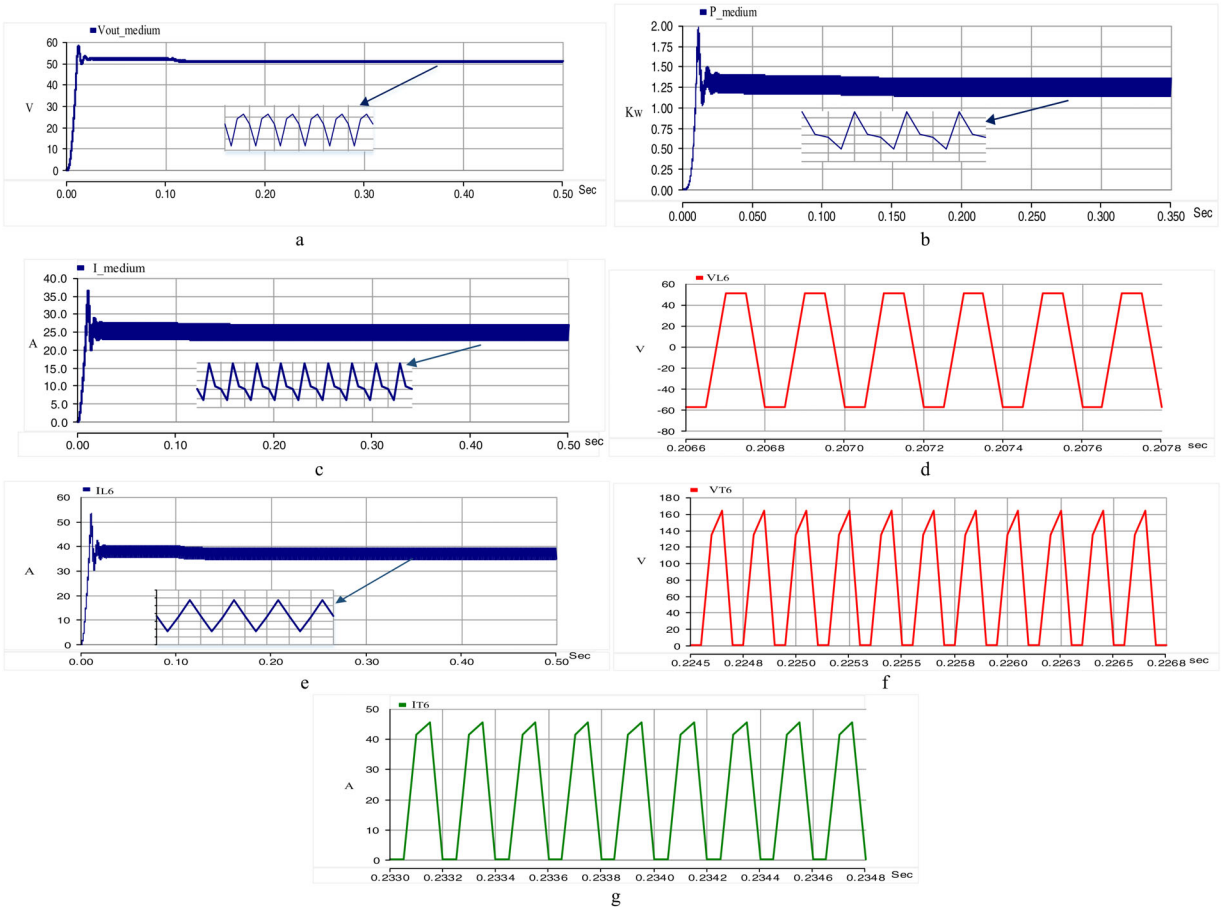

FIGURE 16 (a) Medium-voltage section's voltages in step-change mode, (b) power delivery for the medium-voltage section in step-change mod, c) medium-voltage section's current in step-change mode, (d) L_6's voltage in steady-state mode, (e) L_6's current in step-change mode, (f) T_6's voltage in steady-state mode, (g) T_6's current in steady-state mode

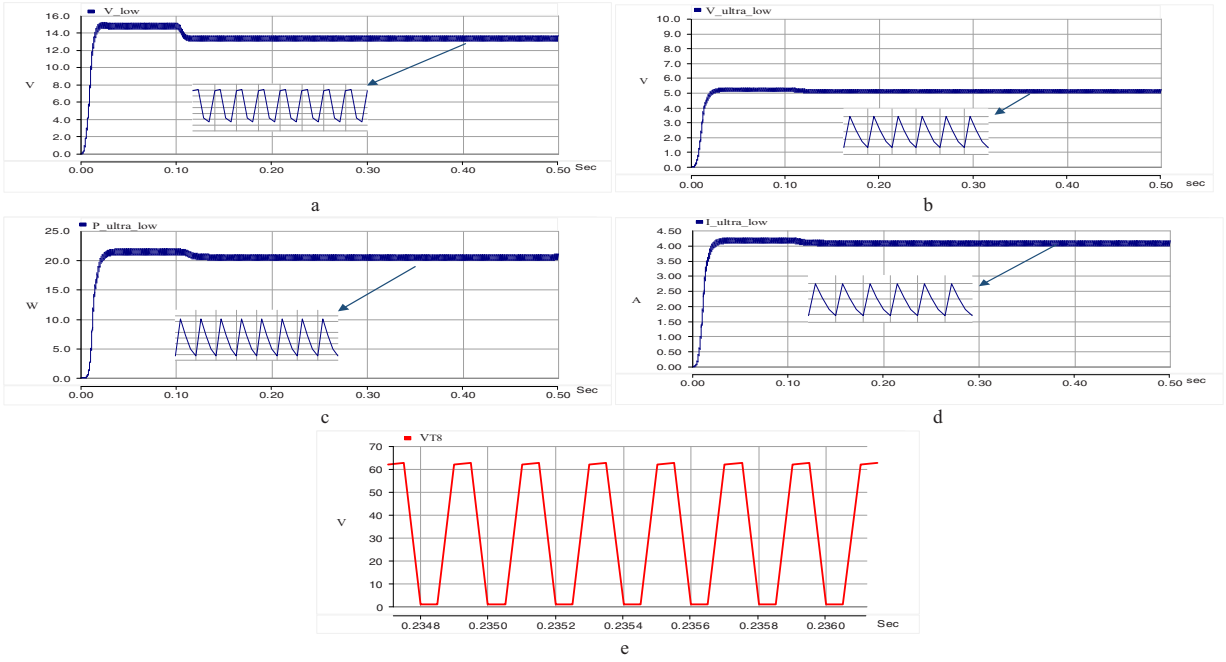

FIGURE 17 (a) Low-voltage section's voltages in step-change mode, (b) ultra-low-voltage section's voltages in step-change mode, (c) power delivery for the ultra-low-voltage section in step-change mode, (d) medium-voltage section's current in step-change mode, (e) T_8's current in steady-state mode

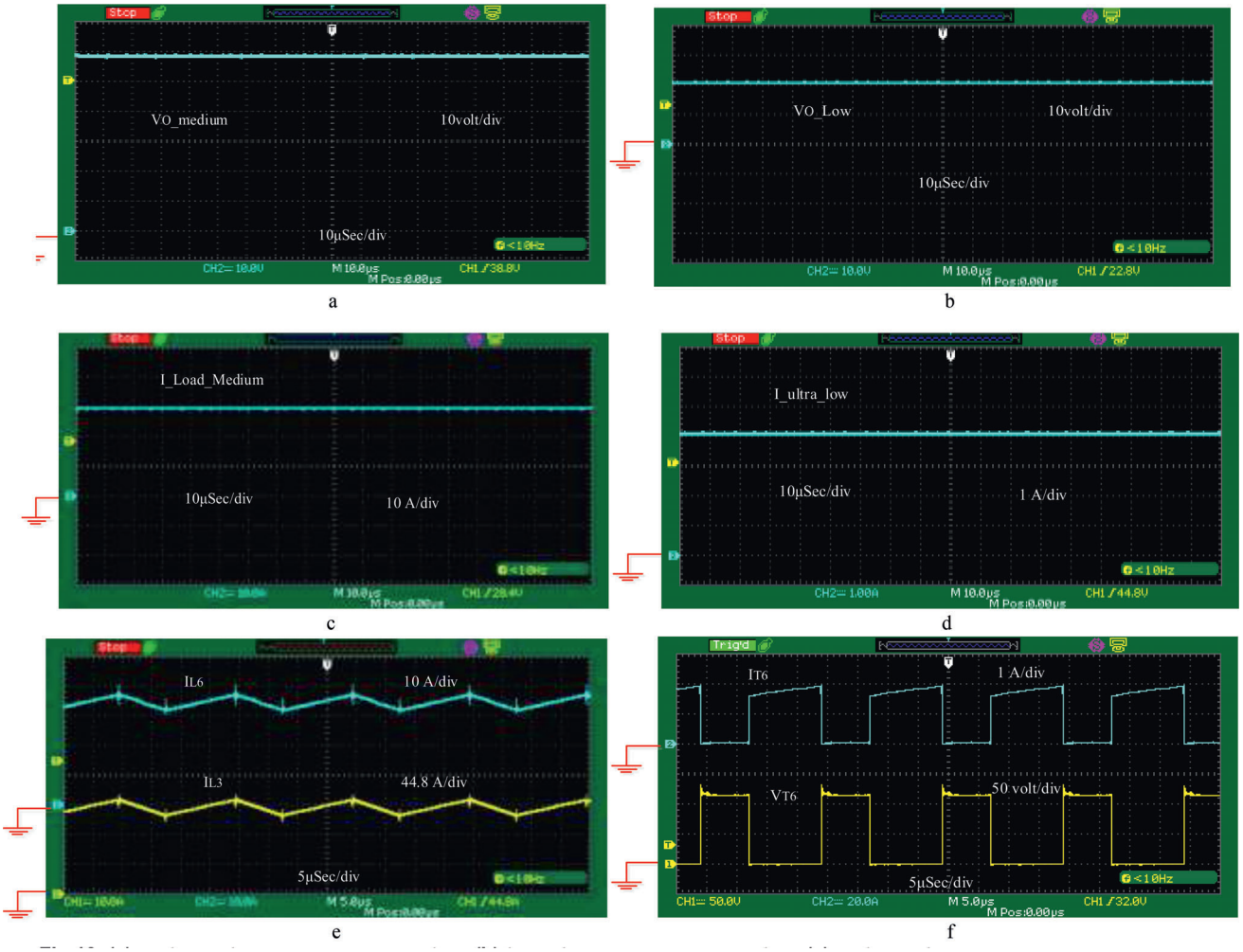

FIGURE 18 (a) Medium-voltage section's out-put voltage, (b) low-voltage section's out-put voltage, (c) medium-voltage section's out-put current, (d) ultra-low-voltage section's out-put current, (e) I_{L6} and I_{L3}'s current, (f) T_6's voltage and current

8 | CONCLUSION

In this study, in order to improve the quality of hybrid systems, the modified power-electronic system is introduced. A three-input/four-output DC–DC system has been proposed.

In addition, to cover the objectives and features of input energy sources, such as charging and discharging of the battery via determining the power of sources, lead to supplying the loads and responding to dynamic load variations. In this study, first, the proposed system's architectures and then the discussion of source management and power distribution in the proposed structure has been studied, and finally, the performance modes of the proposed system have been validated by using PSCAD/EMTDC software and experimental results. The feature of this system is itemised in detail as using renewable and endless resources to generate energy for remote areas of the national grid and its usability, even in urban areas, to be deployed near the national grid. With the capability of producing several voltage levels for different loads, removing buck converters by house electric devices, and determining voltage levels with valid standards, all low power loads are organised in all scenarios so that the control systems and monitoring system may not be cut off.

ORCID

Behnam Zamanzad Ghavidel https://orcid.org/0000-0001-7753-3284
Mohammad Maalandish https://orcid.org/0000-0002-9346-9881
Seyed Hossein Hosseini https://orcid.org/0000-0002-3716-0126
Mehran Sabahi https://orcid.org/0000-0002-4332-6460
Behnam Mohammadi-Ivatloo https://orcid.org/0000-0002-0255-8353

REFERENCES

1. Masoumi, A., et al.: Application of neural network and weighted improved PSO for uncertainty modeling and optimal allocating of renewable energies along with battery energy storage. Appl. Soft Comput. 88, 105979 (2020)

2. Ghavidel, B.Z., Babaei, E., Hosseini, S.H.: An improved three-input DC-DC boost converter for hybrid PV/FC/battery and bidirectional load as backup system for smart home. In: 2019 10th International Power Electronics, Drive Systems and Technologies Conference (PEDSTC), Shiraz, Iran, pp. 533–538 (2019)
3. Wang, C., Nehrir, M.H.: Power management of a stand-alone wind/photovoltaic/fuel cell energy system. IEEE Trans. Energy Convers. 23, 957–967 (2008)
4. Wang, C., et al.: A nonlinear-disturbance-observer-based DC-bus voltage control for a hybrid AC/DC microgrid. IEEE Trans. Power Electron. 29, 6162–6177 (2014)
5. Phattanasak, M., et al.: Control of a hybrid energy source comprising a fuel cell and two storage devices using isolated three-port bidirectional DC–DC converters. IEEE Trans. Ind. Appl. 51, 491–497 (2014)
6. Mohseni, P., et al.: A new high step-up multi-input multi-output DC–DC converter. IEEE Trans. Ind. Electron. 66, 5197–5208 (2018)
7. Maalandish, M., et al.: High step-up DC–DC converter using one switch and lower losses for photovoltaic applications. IET Power Electron. 11, 2081–2092 (2018)
8. Patil, S., Prasad, R.: Design and development of MPPT algorithm for high efficient DC-DC converter for solar energy system connected to grid. In: 2015 International Conference on Energy Systems and Applications, Pune, India, pp. 228–233 (2015)
9. Nejabatkhah, F., et al.: Modeling and control of a new three-input DC–DC boost converter for hybrid PV/FC/battery power system. IEEE Trans. Power Electron. 27, 2309–2324 (2011)
10. Hosseini, S., et al.: Multi-input DC boost converter for grid connected hybrid PV/FC/battery power system. In: 2010 IEEE Electrical Power & Energy Conference, Halifax, NS, Canada, pp. 1–6 25–27 Aug. (2010). DOI: https://doi.org/10.1109/EPEC.2010.5697177
11. Ahrabi, R.R., et al.: A novel step-up multiinput DC–DC converter for hybrid electric vehicles application. IEEE Trans. Power Electron. 32, 3549–3561 (2016)
12. Hosseini, S., et al.: Multi-input dc boost converter supplied by a hybrid PV/Wind turbine power systems for street lighting application connected to the grid. In: 2012 47th International Universities Power Engineering Conference (UPEC), London, UK, pp. 1–6 (2012)
13. Nahavandi, A., et al.: A nonisolated multiinput multioutput DC–DC boost converter for electric vehicle applications. IEEE Trans. Power Electron. 2012 47th International Universities Power Engineering Conference (UPEC), London, UK, 30, 1818–1835 4–7 Sept. (2014). DOI: https://doi.org/10.1109/UPEC.2012.6398632
14. Wu, H., et al.: Topology derivation of nonisolated three-port DC–DC converters from DIC and DOC. IEEE Trans. Power Electron. 28, 3297–3307 (2012)
15. Banaei, M.R., et al.: Non-isolated multi-input–single-output DC/DC converter for photovoltaic power generation systems. IET Power Electron. 7, 2806–2816 (2014)
16. Zhou, L.-W., Zhu, B.-X., Luo, Q.-M.: High step-up converter with capacity of multiple input. IET Power Electron. 5, 524–531 (2012)
17. Varesi, K., et al.: Performance and design analysis of an improved non-isolated multiple input buck DC–DC converter. IET Power Electron. 10, 1034–1045 (2017)
18. Kumar, L., Jain, S.: Multiple-input DC/DC converter topology for hybrid energy system. IET Power Electron. 6, 1483–1501 (2013)
19. Cheng, T., Lu, D.D.-C., Qin, L.: Non-isolated single-inductor DC/DC converter with fully reconfigurable structure for renewable energy applications. IEEE Trans. Circuits Syst. II Express Briefs 65, 351–355 (2017)
20. Taufik, T., and Muscarella, M.: Development of DC house prototypes as demonstration sites for an alternate solution to rural electrification. In: 2016 6th international annual engineering seminar (InAES), (Yogyakarta, Indonesia, pp. 262–2652016)
21. Yoshimi, K., et al.: Practical storage and utilization of household photovoltaic energy by electric vehicle battery. In: 2012 IEEE PES Innovative Smart Grid Technologies (ISGT), Washington, Washington DC, pp. 1–8 (2012)
22. Monteiro, V., Pinto, J., and Afonso, J.L.: Operation modes for the electric vehicle in smart grids and smart homes: Present and proposed modes. IEEE Trans. Veh. Technol. 65, 1007–1020 (2015)

How to cite this article: Zamanzad Ghavidel B, Maalandish M, Hosseini SH, Sabahi M, Mohammadi-Ivatloo B. Design and implementation of an improved power-electronic system for feeding loads of smart homes in remote areas using renewable energy sources. *IET Renew Power Gener.* 2021;15:1–16. https://doi.org/10.1049/rpg2.12001